



NOVEL METHOD TO CLASSIFY AEROSOL PARTICLES ACCORDING TO THEIR MASS-TO-CHARGE RATIO—AEROSOL PARTICLE MASS ANALYSER

Kensei Ehara,^{*†} Charles Hagwood[‡] and Kevin J. Coakley[§]

[†] National Research Laboratory of Metrology, 1-1-4 Umezono, Tsukuba, Ibaraki 305, Japan

[‡] National Institute of Standards and Technology, Gaithersburg, MD 20899, U.S.A.

[§] National Institute of Standards and Technology, Boulder, CO 80303, U.S.A.

(First received 1 August 1995; and in final form 16 October 1995)

Abstract—A new method to classify aerosol particles according to their mass-to-charge ratio is proposed. This method works by balancing the electrostatic and centrifugal forces which act on particles introduced into a thin annular space formed between rotating cylindrical electrodes. Particles having a mass-to-charge ratio lying in a certain narrow range are taken out continuously as an aerosol suspension. A theoretical framework has been developed to calculate the transfer function which is defined as the ratio of the exiting particle flux to the entering particle flux. A similarity rule has been derived which states that a single nondimensional constant determines the shape of the transfer function. To examine the feasibility of the proposed principle, a prototype classifier was constructed, and the mass distribution of monodisperse particles nominally $0.309\ \mu\text{m}$ in diameter was measured. The peak structures corresponding to singly, doubly, and triply charged particles were identified in the experimental spectra. The difference between theory and experiment in the peak location for the singly charged particles was about 6.5% in terms of mass, or 2.3% in terms of diameter.

INTRODUCTION

Various kinds of aerosol classification devices have been developed so far. The basic principle for classification employed in most of these devices involves the balancing of the drag force exerted by the surrounding air on the particles with some constant external force. Examples of such external forces include: the electrostatic force for the electrical aerosol analyzer (Whitby, 1976; Liu *et al.*, 1979) and the differential mobility analyzer (Hewitt, 1957; Knutson and Whitby, 1975); gravity for the horizontal elutriator (Stöber and Flachsbarth, 1971) and the sedimentation cell (Allen and Raabe, 1985; Kousaka *et al.*, 1987); the centrifugal force for the cyclone (Beeckmans, 1979) and various types of aerosol centrifuges such as the conifuge (Tillery, 1979), the cylindrical aerosol spectrometer (Hochrainer, 1971; Abed-Navavdi *et al.*, 1976; Tillery, 1979), the Goetz aerosol spectrometer (Stevenson and Preining, 1960; Gerber, 1979), and the Stöber centrifuge (Stöber, 1976; Tally *et al.*, 1979). Although inertia and the diffusion force are not strictly regarded as external forces, various types of impactors (Marple and Willeke, 1979; Masuda *et al.*, 1979; Prodi *et al.*, 1979) and diffusion batteries (Sinclair *et al.*, 1979) can also be viewed as balancing the drag force with these forces. Since the drag force, which may be described by the Stokes formula modified by the slip correction factor, is determined by the particle diameter, the properties according to which particles are classified with these devices are functions of the particle diameter. The particle properties utilized for this purpose include the electrical mobility, the mechanical mobility, the relaxation time, and the diffusion coefficient.

These properties are important in that they directly govern the particle motion resulting from the relevant external forces. However, being dependent on the particle interaction with the surrounding air, these properties are not purely intrinsic to the particles. Besides, when the particles are not spherical, these properties depend on the particle orientation relative to their movement, and the interpretation and use of these properties often become somewhat

* Author to whom correspondence should be addressed.

complicated. In some situations, therefore, it would be more desirable if one could classify aerosol particles according to their intrinsic properties which do not depend on the particle shapes or orientation, or the properties of the surrounding air. At present, however, only a few such methods are known.

The balance method using a Millikan-type cell, which is actually not for classification but for measurement, can be used to measure the mass-to-charge ratio of an individual aerosol particle. It provides a method for accurate particle size measurement if the particle density is known, and has been applied successfully to the measurement of particle size standards (Kousaka *et al.*, 1987). However, since it is a slow method and deals with only one particle at a time, it is not appropriate for real polydisperse aerosol particles. Also, it is difficult to measure particles smaller than about $0.5\ \mu\text{m}$ because of Brownian motion. The device developed by Masuda and his group (Masuda *et al.*, 1993) who studied the charge distribution of aerosol particles, is essentially a mass-to-charge classifier. The essential part of their device is the vertically oriented planar electrodes. Aerosol particles released at the central line of the top of the electrodes undergo sedimentation in mutually orthogonal electrostatic and gravitational fields, and are collected on slide glasses placed at the bottom of the device and on the electrodes' surfaces. The spatial distribution of the particles deposited onto the slides is measured with a microscope, and from this the distribution of the mass-to-charge ratio is derived. This method is more efficient than the balance method using a Millikan-type cell, but is less precise. The application of this method is restricted to particles larger than about $1\ \mu\text{m}$ due to Brownian motion.

In the present paper, we propose a new method to classify aerosol particles according to their mass-to-charge ratio. This method works by balancing electrostatic and centrifugal forces; the drag force plays only a secondary role. Though the resolution in classification still depends on the particle shape and orientation and the properties of the surrounding air, the location of the center of the classification band is determined solely by the intrinsic particle property. The most notable difference from the methods described above is that in this method the classified particles are obtained as an aerosol suspension. Hence, this method can be used either to generate monodisperse particles, or to measure the mass-to-charge distribution by counting the classified particles by some means such as the condensation nucleus counter or the optical particle counter.

In the following sections, we first develop a theoretical framework to calculate the transfer function. Characteristic features in the classification scheme are analyzed in terms of two different theoretical models of the aerosol velocity distribution in the classifier. On the basis of the principle proposed, we have constructed a prototype classifier. Experimental data collected with this classifier are compared with theory. Though the effects of Brownian motion will be neglected throughout this paper, they are expected to be important for particles smaller than $0.1\ \mu\text{m}$. A stochastic modelling of the classifier which accounts for Brownian motion will be presented in a separate paper (Hagwood *et al.*, 1996).

THEORY

Equation describing the particle trajectory

We begin by considering rotating coaxial cylindrical electrodes. Figure 1 is a schematic drawing of such a device. The inner and outer electrodes rotate at the same angular velocity, ω . The narrow annular space between the electrodes constitutes the space where classification occurs; we will call it the operating space. We will assume that the device is so constructed that when the aerosol is introduced into the operating space, it rotates at the same angular velocity as the electrodes. To ensure this, one may, for example, partition the operating space into some segments perpendicular to the cylinder axis. Voltage V is applied between the electrodes. Let r and z denote the radial and axial coordinates in a cylindrical coordinate system which rotates at the same angular velocity as the electrodes. The origin of the coordinate system is taken in the inlet plane of the operating space. We neglect particle inertia, Brownian motion, the interaction between aerosol particles, and the image

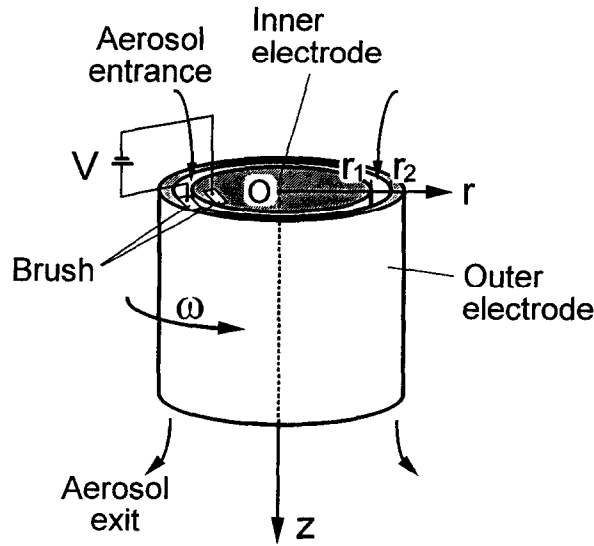


Fig. 1. Schematic diagram of the cylindrical electrodes which classify aerosol particles according to their specific mass given by equation (4).

potential. The equations of motion for a particle having mass m and charge q in the operating space are

$$\frac{m}{\tau} \frac{dr}{dt} = mr\omega^2 - \frac{qV}{r \ln(r_2/r_1)}, \quad (1)$$

$$\frac{m}{\tau} \left[\frac{dz}{dt} - v(r) \right] = 0, \quad (2)$$

where τ is the particle relaxation time, and r_1 and r_2 are the inner and outer radii of the operating space. In equations (1) and (2), the air flow velocity in the operating space is assumed to have only a z -component, $v(r)$, which has no t - or z -dependence. The left-hand sides of these equations represent the drag force which is described by the Stokes formula modified by the slip correction factor, and the first and second terms on the right-hand side of equation (1) represent the centrifugal and electrostatic forces, respectively. We can neglect the Coriolis force, because the primary motion of the particle, which is its axial motion in tandem with the surrounding air, is parallel to the axis of rotation. We consider the case where the product qV is positive and hence the electrostatic and centrifugal forces act in opposite directions. From equation (1), the net external force vanishes when the radial coordinate of the particle is equal to $r(s)$, where

$$r(s) = \sqrt{\frac{V}{s\omega^2 \ln(r_2/r_1)}}. \quad (3)$$

Here s denotes the mass-to-charge ratio given by

$$s = m/q, \quad (4)$$

which we hereafter call the specific mass. In the analysis which follows, we assume that the spacing between the electrodes is much smaller than their radii. This assumption not only simplifies the theoretical analysis, but it is also a condition to be met if we require the resolution in classification to be reasonably high, as will be shown later. This is expressed as

$$\delta/r_c \ll 1, \quad (5)$$

where

$$r_c = (r_1 + r_2)/2, \quad (6)$$

$$\delta = (r_2 - r_1)/2. \quad (7)$$

Under this assumption, we expand the right-hand side of equation (1) in a Taylor series with respect to $(r - r(s))$. The zeroth-order term vanishes by the definition of $r(s)$. Substituting equation (3) into the coefficient of the first-order term and neglecting higher-order terms, we obtain

$$\frac{dr}{dt} = 2\tau\omega^2(r - r(s)). \quad (8)$$

This approximation is valid when analyzing the transfer function which will be introduced shortly, because only those particles for which $|r - r(s)|$ is less than or of the order of δ contribute to the transfer function. Eliminating t from equations (2) and (8) leads to the equation of particle trajectories:

$$\frac{dz}{dr} = \frac{v(r)}{2\tau\omega^2[r - r(s)]}. \quad (9)$$

To express equation (9) in a nondimensional form, we introduce the dimensionless coordinates ρ and ζ given by

$$\rho = (r - r_c)/\delta, \quad (10)$$

$$\zeta = z/L, \quad (11)$$

and velocity distribution of the air flow

$$w(\rho) = v(r)/\bar{v}. \quad (12)$$

Here L is the axial length of the operating space, and

$$\bar{v} = \int_{r_1}^{r_2} v(r)r \, dr / 2\delta r_c \quad (13)$$

is the average flow velocity. Equation (9) can now be rewritten as

$$\frac{d\zeta}{d\rho} = \frac{w(\rho)}{\lambda[\rho - \rho(s)]}, \quad (14)$$

with

$$\rho(s) = [r(s) - r_c]/\delta, \quad (15)$$

$$\lambda = 2\tau\omega^2 L/\bar{v}. \quad (16)$$

The dimensionless constant λ is an important parameter that characterizes the classification performance. It depends on s via τ . From equation (8), $1/(2\tau\omega^2)$ can be regarded as a representative time for a particle to traverse the operating space in the radial direction. On the other hand, L/\bar{v} is the average time for an aerosol to pass through the operating space. Accordingly, λ can be interpreted as the ratio of the axial and radial traversal times.

Transfer function

Suppose that particles having a specific mass s enter the operating space in a spatially uniform concentration n_0 . The total particle flux at the entrance is given by

$$\begin{aligned} F_{\text{in}} &= 2\pi n_0 \int_{r_1}^{r_2} v(r)r \, dr \\ &= 4\pi r_c \delta n_0 \bar{v}. \end{aligned} \quad (17)$$

Let r_0^1 and r_0^h denote, respectively, the initial radial coordinates of the innermost and outermost trajectories of particles which pass through the operating space. The total

particle flux at the exit is given by

$$\begin{aligned}
 F_{\text{out}} &= 2\pi \int_{r_1}^{r_2} v(r) n(r, L) r \, dr \\
 &= 2\pi \int_{r_0^l}^{r_0^h} v(r) n(r, 0) r \, dr \\
 &\approx 2\pi r_c n_0 \int_{r_0^l}^{r_0^h} v(r) \, dr,
 \end{aligned} \tag{18}$$

where $n(r, z)$ is the particle concentration at a point (r, z) . The last line in this equation is an approximate expression valid under condition (5). In analogy to the theoretical analysis of the differential mobility analyzer by Knutson and Whitby (1975), we introduce the transfer function which in our case is defined as $F_{\text{out}}/F_{\text{in}}$. Its explicit form is derived from equations (17) and (18) to be

$$t(s) = \frac{1}{2} \int_{\rho_0^l}^{\rho_0^h} w(\rho) \, d\rho, \tag{19}$$

where ρ_0^l and ρ_0^h are the nondimensional coordinates corresponding to r_0^l and r_0^h , respectively.

MODEL CALCULATIONS

Unlike the differential mobility analyzer, the transfer function for the present classifier depends on the structure of the flow field, as equation (19) shows. This dependence comes from the fact that the field of the centrifugal force is not divergent-free, and, therefore, the function analogous to the stream function for the flow field, or to the electric flux function as termed by Knutson and Whitby (1975) for the electrostatic field, cannot be defined for the centrifugal force field.

We consider two models for $w(\rho)$ below. One is so simple that we can obtain an approximate analytical solution for the transfer function. This model may not be satisfactory for the detailed analysis of the classifier performance, but it is useful for obtaining an intuitive understanding of the classification mechanism. The other model contains the essential features of a real classifier, and is expected to provide theoretical predictions that can be compared directly with the experiment. Calculation of the transfer function in the latter model requires numerical computation.

Uniform flow model

In this model, we assume that $w(\rho)$ is uniform over ρ , namely that

$$w_u(\rho) = 1. \tag{20}$$

Using equation (20), we can solve equation (14) easily to get

$$\rho - \rho(s) = [\rho_0 - \rho(s)] \exp(\lambda \zeta), \tag{21}$$

where ρ_0 is the initial value of ρ . The parameter $\rho(s)$ indicates the point of unstable equilibrium in the ρ -direction motion. As shown in Fig. 2, we can identify five regions of $\rho(s)$ each of which corresponds to a different trajectory pattern. In Regions (B), (C), and (D) shown in Fig. 2, particles in the hatched areas pass through the operating space. Particles outside these areas will be deposited onto the surfaces of the electrodes. In Region (C), $\rho(s)$ is located between the electrode surfaces; that is

$$-1 < \rho(s) < 1 \quad [\text{Region (C)}]. \tag{22}$$

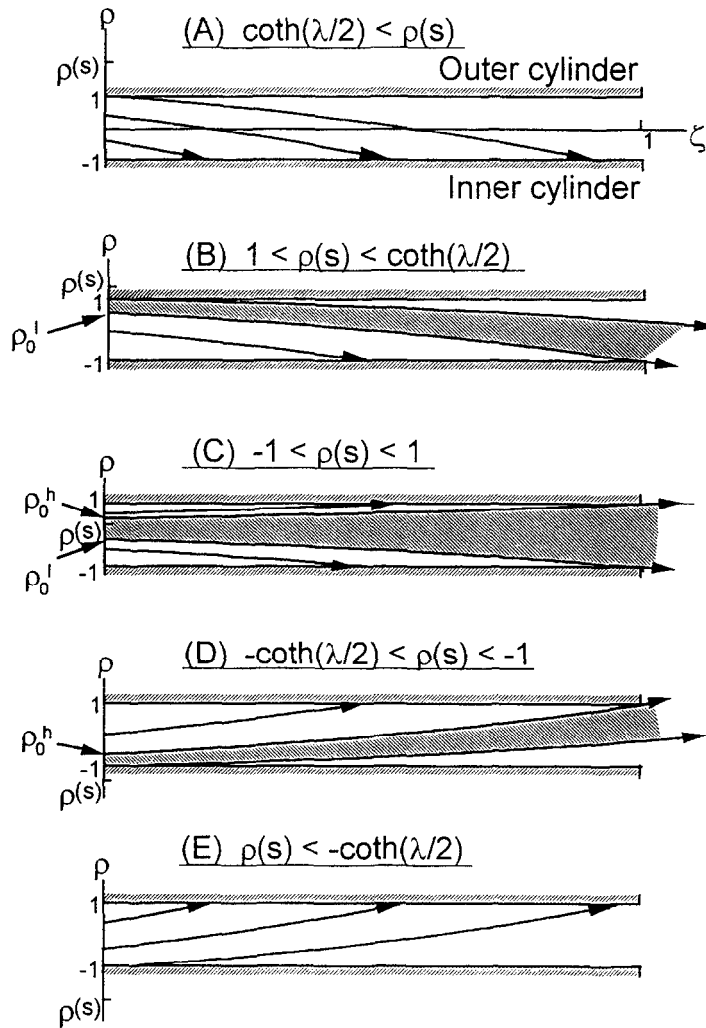


Fig. 2. Various cases of the trajectory patterns. Particles in the hatched areas pass through the operating space.

In this region, ρ_0^l and ρ_0^h are the initial values of ρ of the particles which pass the points (ρ, ζ) given by $(-1, 1)$ and $(1, 1)$, respectively. From equation (21), these are

$$\rho_0^l = (1 - e^{-\lambda})\rho(s) - e^{-\lambda}, \quad (23)$$

$$\rho_0^h = (1 - e^{-\lambda})\rho(s) + e^{-\lambda}, \quad (24)$$

Substituting these expressions into equation (19), we obtain

$$t(s) = e^{-\lambda} \quad [\text{Region (C)}]. \quad (25)$$

In Region (B), the inward electrostatic force is slightly larger in magnitude than the outward centrifugal force. As is obvious from Fig. 2, ρ_0^h is equal to unity, and as for ρ_0^l , equation (23) still applies. Hence, we have

$$t(s) = \{[1 - \rho(s)] + [1 + \rho(s)]e^{-\lambda}\}/2 \quad [\text{Region (B)}]. \quad (26)$$

The condition that ρ_0^l should be located inside the outer electrode surface imposes the upper limit to $\rho(s)$, yielding

$$1 < \rho(s) < \coth(\lambda/2) \quad [\text{Region (B)}] \quad (27)$$

Similarly, for Region (D) we have

$$-\coth(\lambda/2) < \rho(s) < -1 \quad [\text{Region (D)}] \quad (28)$$

and the transfer function is calculated to be

$$t(s) = \{[1 + \rho(s)] + [1 - \rho(s)]e^{-\lambda}\}/2 \quad [\text{Region (D)}]. \quad (29)$$

When $\rho(s)$ is larger than $\coth(\lambda/2)$ [Region (A)], or smaller than $-\coth(\lambda/2)$ [Region (E)], it is obvious that $t(s)$ vanishes.

Let s_c denote the specific mass corresponding to the center of Region (C), that is $\rho(s_c) = 0$. The solution obtained from equations (3) and (15) is

$$s_c = \frac{V}{r_c^2 \omega^2 \ln(r_2/r_1)}. \quad (30)$$

To determine the transfer function, we have to solve inequalities (22), (27), and (28) for s . Let s_1^- , s_1^+ , s_2^- , and s_2^+ denote the values of s for which $\rho(s)$ is equal to $\coth(\lambda/2)$, $-\coth(\lambda/2)$, 1, and -1 , respectively. The solutions for s_2^- and s_2^+ are easily obtained to be

$$s_2^\pm = \frac{s_c}{(1 \mp \delta/r_c)^2}. \quad (31)$$

On the other hand, s_1^- and s_1^+ cannot be solved for analytically, because λ depends on s in a rather complicated manner through τ . If the range from s_1^- to s_1^+ is so narrow that we can neglect the variation of $\coth(\lambda/2)$ in this range, we may replace λ with its value at $s = s_c$, which will be denoted by λ_c . With this approximation, s_1^- and s_1^+ are obtained analytically to be

$$s_1^\pm = \frac{s_c}{[1 \mp (\delta/r_c)\coth(\lambda_c/2)]^2}. \quad (32)$$

Also, we replace λ in equations (25), (26), and (29) with λ_c in the same manner. Under condition (5), the expressions (30), (31), and (32) can be further simplified to yield

$$s_c \approx V/(2r_c \delta \omega^2), \quad (33)$$

$$s_1^\pm \approx s_c(1 \pm 2\delta/r_c), \quad (34)$$

$$s_2^\pm \approx s_c[1 \pm 2(\delta/r_c)\coth(\lambda_c/2)]. \quad (35)$$

For equation (35) to be valid, it is required in addition that $\coth(\lambda_c/2)$ is at most of the order of unity. This requirement is equivalent to insisting that the resolution in the classification be reasonably high, as seen in equation (36) below. The transfer function thus determined is shown in Fig. 3. It has the shape of a symmetric trapezoid whose center is located at s_c . The base width relative to s_c , which is a measure of the resolution in the classification, is given by

$$\frac{\Delta s}{s_c} = \frac{4\delta}{r_c} \coth\left(\frac{\lambda_c}{2}\right), \quad (36)$$

and its height is $\exp(-\lambda_c)$. In the following, we will refer to λ_c as the resolution parameter, and the range from s_1^- to s_1^+ as the specific mass band.

Although it is also possible to take the s -dependence of λ within the specific mass band fully into consideration by means of numerical calculation, we will not do so in the present model. It will be taken into consideration in the subsequent model.

Parabolic flow model

The steady-state solution for the axisymmetric velocity distribution of an incompressible viscous fluid flowing between two coaxial cylinders is well-known (Landau and Lifshitz, 1963). Under condition (5), it can be written to a good approximation as

$$w_p(\rho) = 3(1 - \rho^2)/2. \quad (37)$$

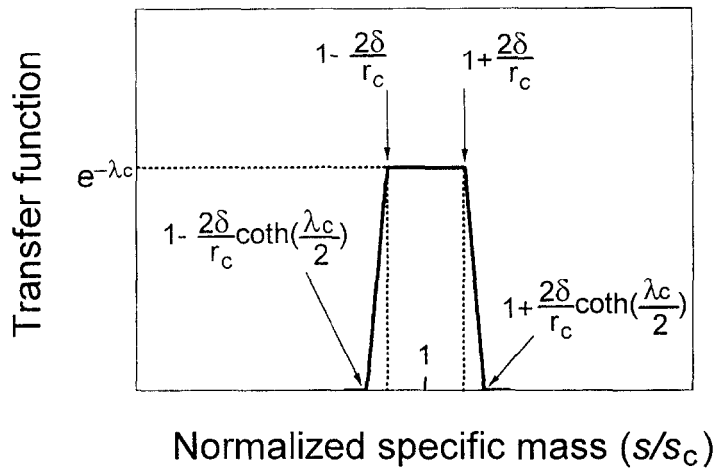
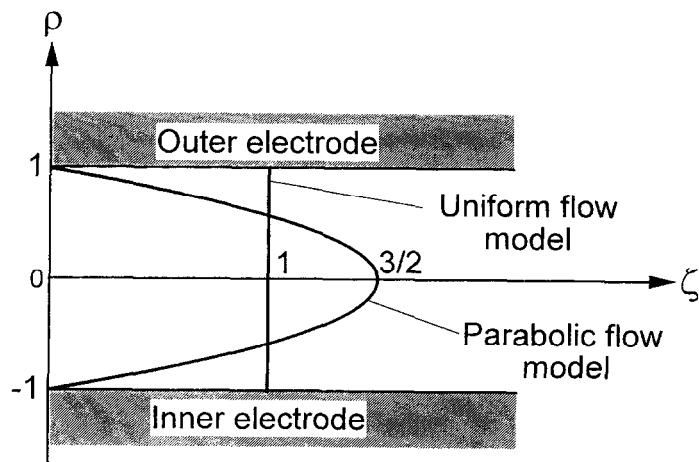
Fig. 3. Transfer function, $t(s)$, in the uniform flow model.

Fig. 4. Velocity distributions of the air flow between the electrodes in the uniform and parabolic flow models.

This is similar in form to the equation describing the flow between two parallel plates. The factor of $3/2$ ensures that $w_p(\rho)$ gives the same total flow rate as $w_u(\rho)$. Figure 4 compares $w_u(\rho)$ and $w_p(\rho)$. In a real device, it is expected that there is a transition region near the inlet where the aerosol flow is not described by $w_p(\rho)$. The length of such a region is known to be about $0.08\delta Re$ (Schlichting, 1962), where Re is the Reynolds number referred to the width of the operating space. For the parameter values given later in Table 1 and an aerosol flow rate of 1 l/min, the Reynolds number is of the order of unity. Accordingly, the length of the transition region is expected to be much shorter than L , so that its effect on the classification performance can be neglected.

In this model, the solution to equation (14) is given by

$$\zeta = \frac{3}{2\lambda} [1 - \rho^2(s)] \ln \left[\frac{\rho - \rho(s)}{\rho_0 - \rho(s)} \right] - \frac{3}{4\lambda} \{ [\rho + \rho(s)]^2 - [\rho_0 + \rho(s)]^2 \}. \quad (38)$$

Whenever the explicit expression for the s -dependence of λ is required in the subsequent analysis, we will assume that the particle is a sphere of density 1 g cm^{-3} and that it carries unit elementary charge, unless otherwise stated. This enables us to relate s with the particle

diameter, d_p , which appears in the expression for the relaxation time given by

$$\tau = \frac{mC(d_p)}{3\pi\eta d_p}. \quad (39)$$

Here η is the viscosity coefficient of air, and $C(d_p)$ is the slip correction factor. In this paper, we use $\eta = 1.87 \times 10^{-5}$ Pa s and the expression for $C(d_p)$ given by Allen and Raabe (1985) which is

$$C(d_p) = 1 + \frac{2l}{d_p} \left[1.142 + 0.558 \exp\left(\frac{-0.999 d_p}{2l}\right) \right], \quad (40)$$

where l is the mean free path of air molecules for which we take $l = 0.0664 \mu\text{m}$. Under this assumption, particle trajectories were calculated from equation (38) for various values of $\rho(s)$. The results are shown in Fig. 5. In this calculation, the device parameters given in Table 1 and a total aerosol flow rate of 1.0 l/min were used, and it was assumed that $V = 1000$ V and $\omega = 3000$ RPM. This choice of the parameter values results in λ_c equal to 1.12.

A distinct difference in the trajectory patterns between the uniform and the parabolic flow models, which is not directly evident in Figs 2 and 5, is found when we consider the distance a particle starting at either surface of the electrodes moves in the ζ -direction until it reaches the other surface. Figures 6 and 7 compare this distance yielded by the two models, where $\lambda\zeta(\rho = -1; \rho_0 = 1)$ and $\lambda\zeta(\rho = 1; \rho_0 = -1)$ calculated from equations (21) and (38) for various values of V are shown. Since the outlet of the operating space corresponds to $\zeta = 1$, the intersection point of λ and $\lambda\zeta(\rho = -1; \rho_0 = 1)$ in these figures determines the value of s_1^- for each value of V . Similarly, the intersection point of λ and $\lambda\zeta(\rho = 1; \rho_0 = -1)$ yields s_1^+ for each value of V . A remarkable feature in Fig. 7 is that $\lambda\zeta(\rho = -1; \rho_0 = 1)$ and $\lambda\zeta(\rho = 1; \rho_0 = -1)$ never exceed 3.0 in the parabolic flow model. This feature can be confirmed using equation (38) by examining $\lambda\zeta$ in the limit that $\rho(s)$ approaches the electrode surfaces from outside of the operating space. Consequently, for relatively large values of V , the curves for $\lambda\zeta(\rho = -1; \rho_0 = 1)$ and $\lambda\zeta(\rho = 1; \rho_0 = -1)$ do not intersect the curve for λ , and hence s_1^- and s_1^+ do not exist. In such situations, Regions (B) and (D) in Fig. 5 do not occur, and the transfer function vanishes whenever $\rho(s)$ is located outside of the operating space.

The threshold, s_1^- , if it exists, should satisfy equation (38) with substitution $\rho_0 = 1$ and $(\rho, \zeta) = (-1, 1)$, which implies that

$$\lambda(s_1^-) = \frac{3}{2} [1 - \rho^2(s_1^-)] \ln \left[\frac{\rho(s_1^-) + 1}{\rho(s_1^-) - 1} \right] + 3\rho(s_1^-). \quad (41)$$

Here the s -dependence of λ is emphasized by writing $\lambda(s)$. Similarly, s_1^+ satisfies equation (38) with $\rho_0 = -1$ and $(\rho, \zeta) = (1, 1)$, which implies that

$$\lambda(s_1^+) = \frac{3}{2} [1 - \rho^2(s_1^+)] \ln \left[\frac{\rho(s_1^+) - 1}{\rho(s_1^+) + 1} \right] - 3\rho(s_1^+). \quad (42)$$

These equations can only be solved numerically. On the other hand, s_2^- and s_2^+ are independent of the flow model, and equations (31) and (34) still apply in the parabolic flow model.

From equations (19) and (37), the transfer function in the parabolic flow model is

$$t(s) = (\rho_0^h - \rho_0^l) [3 - (\rho_0^h)^2 - \rho_0^h \rho_0^l - (\rho_0^l)^2] / 4. \quad (43)$$

To obtain ρ_0^l and ρ_0^h in Region (C), we substitute $(\rho, \zeta) = (-1, 1)$ and $(1, 1)$, respectively, in equation (36), and solve for ρ_0 numerically. This procedure applies also to ρ_0^l in Region (B) and ρ_0^h in Region (D), if these regions exist. On the other hand, the values of ρ_0^h in Region (B) and ρ_0^l in Region (D) are 1 and -1 , respectively, as is obvious from Fig. 5.

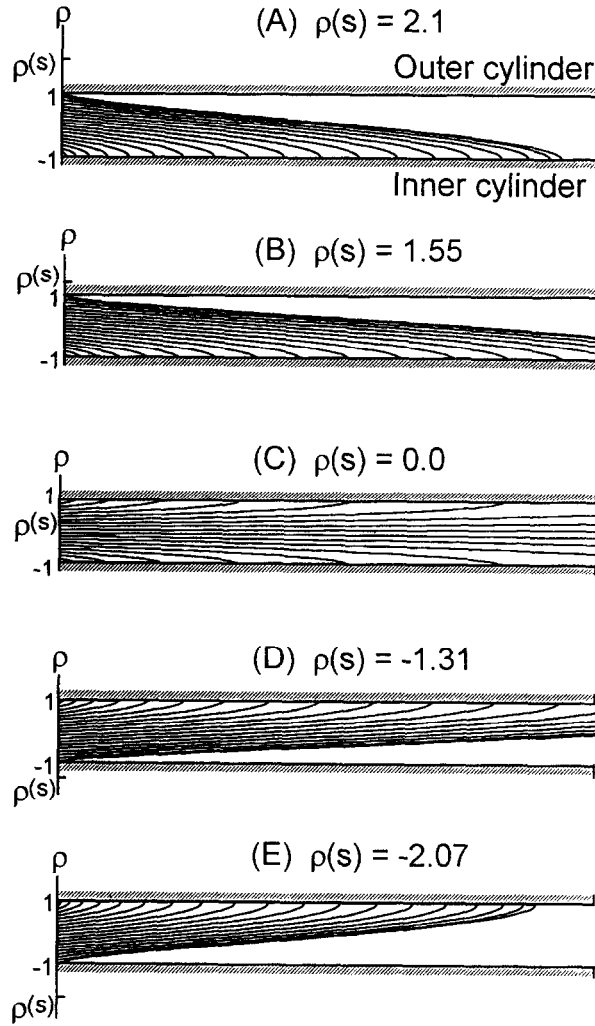


Fig. 5. Particle trajectories for various values of $\rho(s)$ in the parabolic flow model. The resolution parameter, λ_c , was assumed to be 1.12 throughout.

The transfer functions calculated in this way are shown in Fig. 8. For comparison, the transfer functions in the uniform flow model are shown, too. As will be verified in the following section, the shape of the transfer function is determined mainly by λ_c , and does not depend significantly on the individual design and operation parameters. In Fig. 8(a) where λ_c is much smaller than unity, the transfer function looks like a skewed trapezoid. As λ_c becomes larger, the symmetry of the trapezoid tends towards being restored, and the two models result in similar shapes as is seen in Figs 8(b), (c), (e), and (f). When λ_c exceeds unity, the parabolic flow model gives narrower transfer functions with higher peak height than the uniform flow model. This occurs, because in the parabolic flow model the axial motion of particles in the neighborhood of the electrode surfaces is inert, which in effect narrows the width of the operating space. As λ_c increases further, the transfer function eventually assumes a Gaussian-like shape as is observed in Fig. 8(h).

When the transfer function is noticeably asymmetric, the meaning of s_c is not so clear. In most cases shown in Fig. 8, however, it is fairly symmetric, and we can think of s_c as representing the center of the specific mass band. In Fig. 9, s_c is calculated as a function of the applied voltage. The device parameters given in Table 1 were used in this calculation. The particle mass and diameter derived from s_c are also shown as separate scales in Fig. 9. The calculated relative width, $\Delta s/s_c = (s_1^+ - s_1^-)/s_c$, is given in Fig. 10. When s_1^+ and s_1^- do not exist, s_2^+ and s_2^- were used instead. Note that the relative width by diameter, $\Delta d_p/d_{pc}$, is

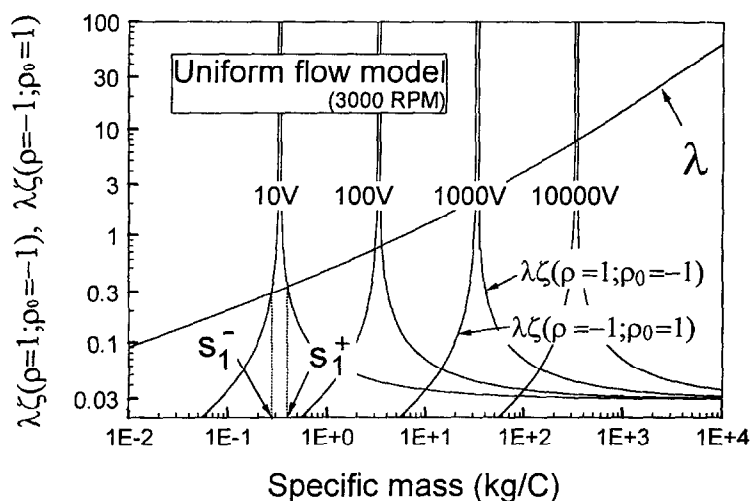


Fig. 6. Values of $\lambda\zeta(\rho = 1; \rho_0 = -1)$ and $\lambda\zeta(\rho = -1; \rho_0 = 1)$ as functions of specific mass for various voltage settings calculated in the uniform flow model. The device parameters given in Table 1 were used in the calculation. For each voltage setting, the leftmost curve is for $\lambda\zeta(\rho = -1; \rho_0 = 1)$ and the rightmost curve is for $\lambda\zeta(\rho = 1; \rho_0 = -1)$.

about one-third of $\Delta s/s_c$. Hence, a magnitude of $\Delta s/s_c$ as large as 1.0 would still give an acceptable resolution in terms of particle diameter. Figures 9 and 10 demonstrate that the present method can be applied to particles whose sizes are in practically important ranges, subject to a feasible choice of design and operation parameters.

Similarity rule

Figure 8 suggests that the shapes of transfer functions for similar values of λ_c resemble one another. In this section, we examine such a similarity with respect to λ_c .

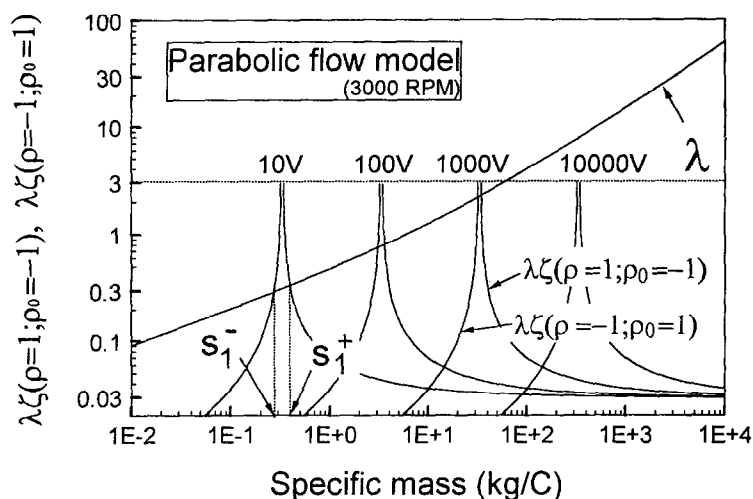


Fig. 7. Values of $\lambda\zeta(\rho = 1; \rho_0 = -1)$ and $\lambda\zeta(\rho = -1; \rho_0 = 1)$ as functions of specific mass for various voltage settings calculated in the parabolic flow model. For details, see Fig. 6.

* Since d_p is proportional to $s^{1/3}$, the logarithmic derivative yields $\Delta d_p/d_{pc} = 1/3(\Delta s/s_c)$ for infinitesimally small Δd_p and Δs . When Δd_p and Δs are finite, this relationship is approximate.

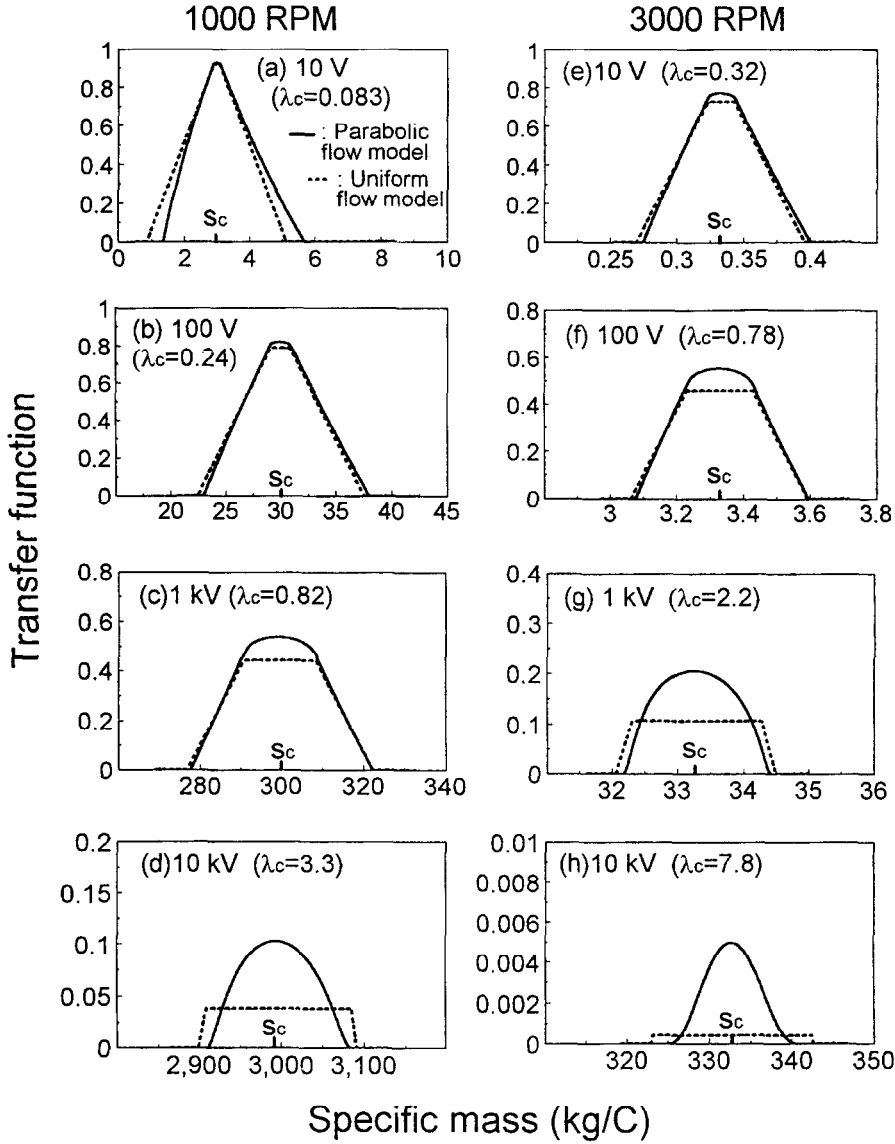


Fig. 8. Transfer functions in the parabolic (solid lines) and uniform (broken lines) flow models for various voltage settings and rotational velocities. The device parameters given in Table 1 were used in the calculation. Figures from (a) to (d) are for 1000 RPM and (e) to (h) are for 3000 RPM. Note that the vertical scales are not identical.

Equation (14) indicates that for any situation where both $\lambda(s)$ and $\rho(s)$ are equal, the trajectory patterns are identical. For any two values of s , it is always possible to realize this similarity by choosing appropriate values for the parameter set $\{\omega, V, L, \bar{v}, \dots\}$. However, for the transfer functions in two different instances to be similar, it is required that both $\lambda(s)$ and $\rho(s)$ behave identically for both instances.

The function $\rho(s)$ can be rewritten as

$$\rho(s) = \frac{r_c}{\delta} \left(\sqrt{\frac{s_c}{s}} - 1 \right), \quad (44)$$

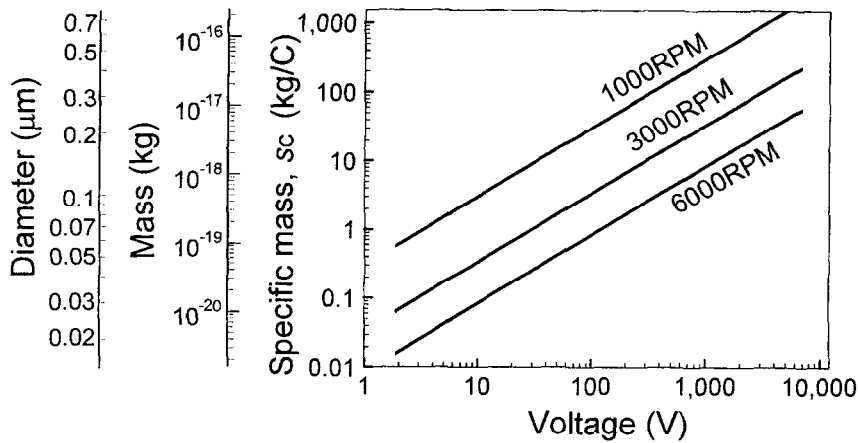


Fig. 9. Center of the specific mass, s_c , as a function of the applied voltage for various rotational velocities. The scales for the particle mass and the diameter for the corresponding s_c are also given under the assumption that the particle carries unit elementary charge and is a sphere of density 1 g cm^{-3} .

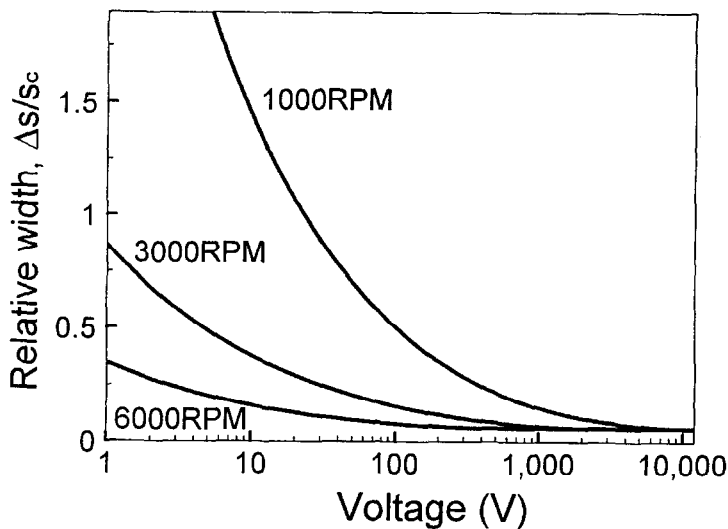


Fig. 10. The specific mass band relative width $\Delta s/s_c$ as a function of the applied voltage. The device parameters given in Table 1 and a total aerosol flow rate of 0.51 min^{-1} were assumed.

and hence it is a function of s/s_c , with r_c/δ being a scaling factor. To examine how $\lambda(s)$ behaves as a function of s/s_c , we calculate $\lambda(s)$ for three different values of s_c , with the parameter set being chosen to give the same value of λ_c for each value of s_c . The result is shown in Fig. 11, where λ_c was chosen arbitrarily to be 1.0. We notice that $\lambda(s)$ as a function of s/s_c changes little for three widely different values of s_c . This suggests that the transfer functions for the same value of λ_c are approximately equal when expressed as functions of s/s_c . That this is in fact true is seen in Fig. 12, where we find that the transfer functions in the parabolic flow model for the three values of s_c coincide within the thickness of the plotted lines for constant λ_c . For values of λ_c larger than those shown in Fig. 12, this observation is even more accurate, because the width of the specific mass band is narrower.

In Fig. 13, the relative width of the transfer function, $\Delta s/s_c$, is plotted as a function of λ_c . The three curves in Fig. 10 are not distinguishable in Fig. 13. They approach $4\delta/r_c$ asymptotically as λ_c increases. Note that since Δs is the base width, little difference is observed between the uniform and parabolic flow models in Fig. 13. The maximum transfer

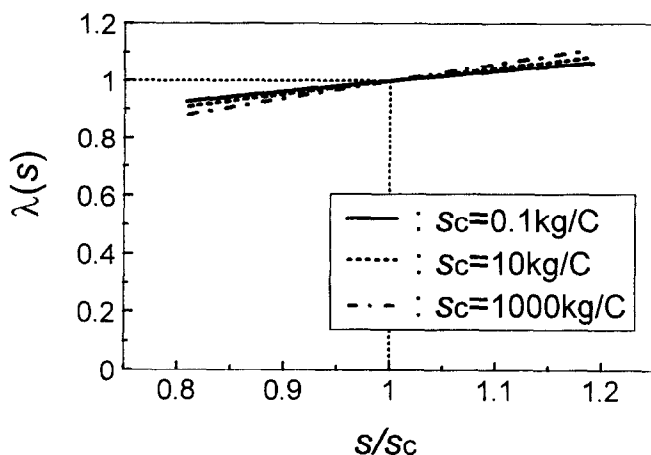


Fig. 11. Behavior of the nondimensional parameter $\lambda(s)$ as a function of s/s_c for various values of s_c . The parameter set is chosen so that $\lambda(s_c)$ is equal to 1.0 for all values of s_c .

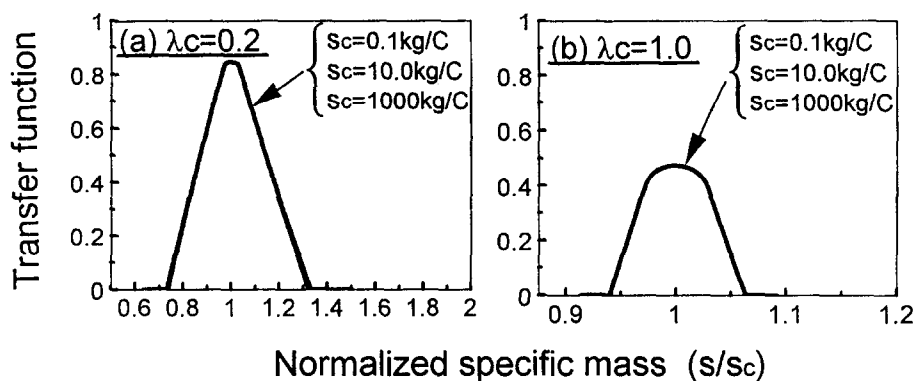


Fig. 12. Transfer functions in the parabolic flow model for the three sets of parameters which give the same values of λ_c for three different values of s_c . The three transfer functions nearly coincide both in (a) and (b).

function height, $t(s_c)$, as a function of λ_c is shown in Fig. 14. The parabolic flow model gives a larger $t(s_c)$ than the uniform flow model especially for large λ_c .

Figures 13 and 14 give an indication of an appropriate choice for λ_c in real applications. If one requires $\Delta d_p/d_{pc}$ to be smaller than 0.4, for example, which is equivalent to $\Delta s/s_c$ being smaller than about 1.2, then λ_c should be larger than 0.1. On the other hand, if λ_c is too large, only a small fraction of entering particles will come out, which will usually be undesirable. If one requires $t(s_c)$ to be larger than 0.1, λ_c should be smaller than about 3 by Fig. 14. Consequently, $0.1 \leq \lambda_c \leq 3$ would be an appropriate choice for λ_c in typical applications.

EXPERIMENTAL VERIFICATION

We have constructed a prototype classifier based on the principles described above. As is shown schematically in Fig. 15, the coaxial cylindrical electrodes constitute the operating space whose dimensions are summarized in Table 1. An aerosol drawn through the inlet tube flows outwardly into the thin topmost space, and enters the operating space. Four thin

Table 1. Summary of the device parameters of the prototype aerosol particle mass analyzer

r_1 (outer radius of the inner electrode)	100 mm
r_2 (inner radius of the outer electrode)	103 mm
L (vertical length of the electrodes)	200 mm

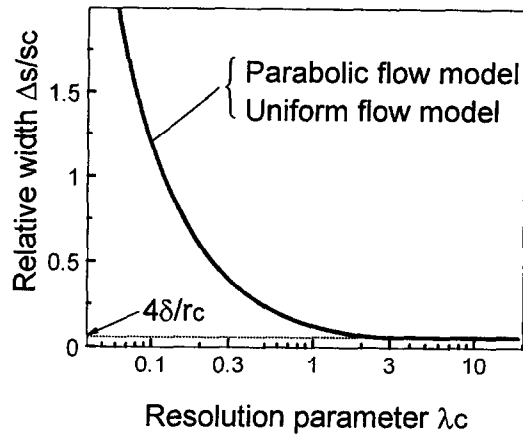


Fig. 13. The transfer function relative width $\Delta s/s_c$ as a function of the resolution parameter λ_c . Results for the parabolic and uniform flow models nearly coincide.

plastic partitions parallel to the axis, not shown in Fig. 15, are inserted between the electrodes to ensure that the aerosol rotates at the same velocity as the electrodes. The aerosol exiting the operating space flows inwardly at the bottommost space, and is finally taken out via the outlet tube located at the rotation axis. The high voltage is applied through the brushes which make electrical contact between the rotating and stationary parts. For the device parameters given in Table 1, δ/r_c is equal to about 0.015, and hence condition (5) is safely satisfied.

To examine the performance of the prototype, we have measured the mass distribution of monodisperse polystyrene latex (PSL) spheres nominally $0.309 \mu\text{m}$ in diameter, produced by JSR Co. Figure 16 shows schematically the setup used for this experiment. An aerosol generated by atomizing a PSL suspension was passed through a charge neutralizer utilizing ^{241}Am prior to classification. The particle concentration in the aerosol leaving the classifier was measured with a laser particle counter (KC-18, Rion Co., Tokyo) for various voltage settings. Two measurements were made: one with the charge neutralizer and one without. The rotational velocity was fixed at 1000 RPM. The temporal stability of the particle concentration in the entering aerosols was also monitored with the particle counter. The results of our measurements are given in Fig. 17. Each experimental spectrum is normalized to the maximum in the region of 300 V. The arrows labelled $q = 1, 2$ and 3 in Fig. 17 indicate the theoretically predicted peak locations corresponding to singly, doubly, and triply charged particles, respectively. A particle density of 1.054 g cm^{-3} , the value provided

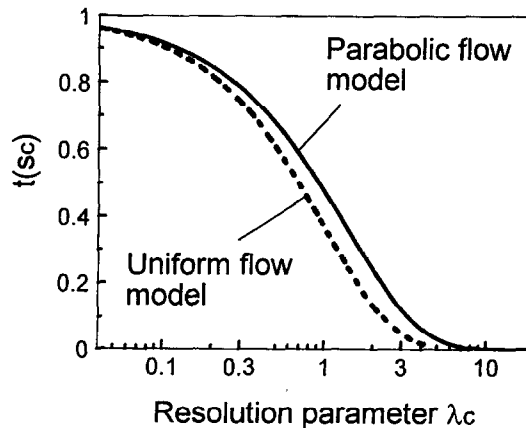


Fig. 14. Maximum height of the transfer function in the uniform and parabolic flow models as functions of λ_c .

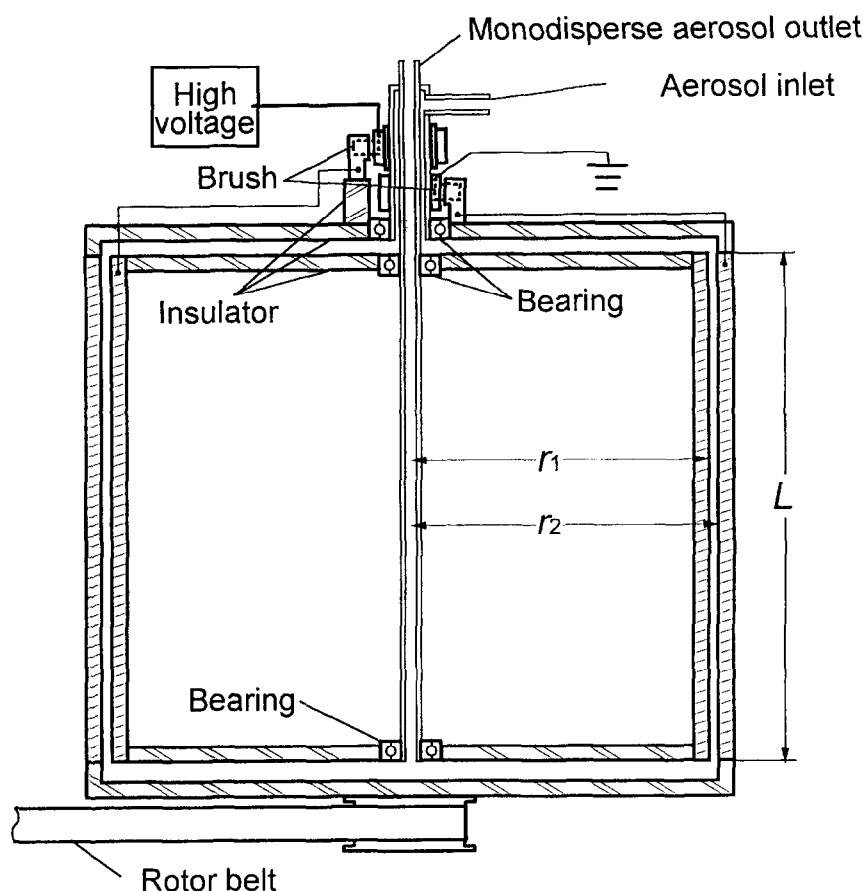


Fig. 15. Schematic diagram of the prototype aerosol particle mass analyzer.

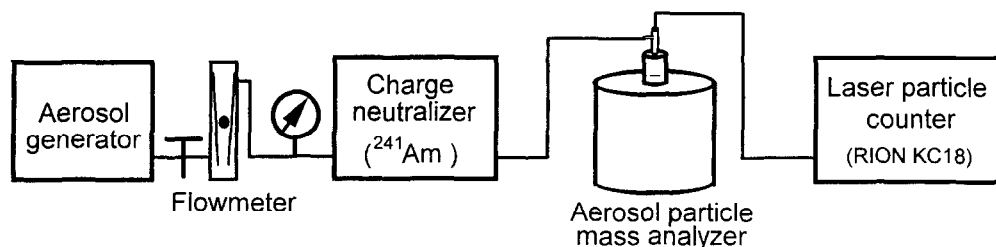


Fig. 16. Experimental setup for measuring the mass distribution of monodisperse polystyrene latex spheres.

by the manufacturer of the PSL spheres, was used in the calculation. Although the maxima for doubly and triply charged particles in the absence of the charge neutralizer are not well resolved, the other peak positions agree fairly well with the theoretical predictions.

The concentration of the exiting particles as a function of voltage, $n(V)$, is given by

$$n(V) = \int f(s)t(s) ds. \quad (45)$$

Here, $f(s)$ is the specific mass distribution of the aerosol particles before classification, and is assumed to be proportional to the δ -function, for simplicity. As a result of air leaks probably through the bearings, the exact aerosol flow rate in the operating space could not be determined. For instance, when the flow rate of the entering aerosol was 1.1 l min^{-1} , the flow rate measured at the outlet was around 0.7 l min^{-1} . So we took the average of

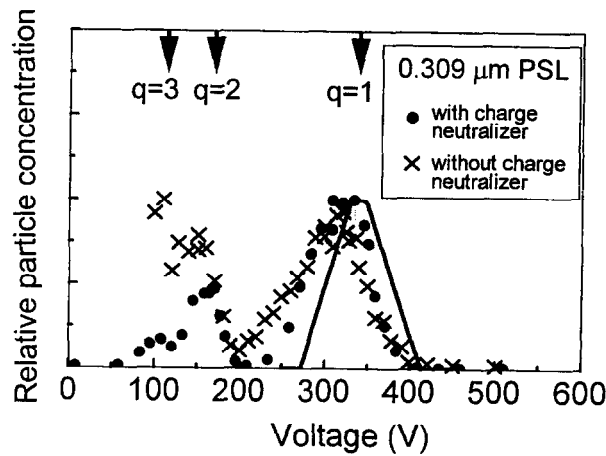


Fig. 17. Experimental spectra for $0.309\ \mu\text{m}$ PSL spheres. The arrows indicate the theoretical predictions of the peak positions and the solid line is for a theoretically calculated spectrum.

$0.9\ \text{l min}^{-1}$ to obtain a rough estimate of the flow rate in the operating space, and we used this value to calculate $n(V)$ for singly charged particles. The solid curve in Fig. 17 shows the result of this calculation which used $t(s)$ in the parabolic flow model. We note that the theory predicts a slightly larger mass distribution than is observed in the experiment. According to equation (30), the experimental peak position, $318\ \text{V}$, corresponds to $m = 1.53 \times 10^{-17}\ \text{kg}$, or $d_p = 0.302\ \mu\text{m}$. So the relative disagreement between theory and experiment is about 6.5% in terms of mass, or 2.3% in terms of diameter.

Due to the four partitions in the operating space, the velocity of the aerosol flow is expected to depend on the azimuthal angle, ϕ . If the ϕ -dependence of the average velocity, $\bar{v}(\phi)$, were known, it could be accounted for by considering a local transfer function $t(s, \phi)$, and integrating it over ϕ to obtain the total transfer function. Although the inhomogeneity of \bar{v} may lead to a variation in the width of the transfer function with ϕ , its center, s_c , will not be affected. Thus, this inhomogeneity is expected to have only a minor effect on $n(V)$. It should also be noted that the prediction of the maxima's positions is not affected by the absence of an exact value for the total aerosol flow rate.

CONCLUSIONS

A method to classify aerosol particles according to their specific mass has been proposed. Since classified particles are obtained as an aerosol suspension, the classification device based on this method may be regarded as the mass-to-charge counterpart of the differential mobility analyzer; the latter is essentially a classifier of the diameter-to-charge ratio. Unlike the differential mobility analyzer, the transfer function for this method depends on the detailed form of the velocity distribution of the aerosol flow in the operating space. We considered two models for the velocity distribution. The uniform flow model leads to an analytical expression for the transfer function which has the shape of a symmetric trapezoid. The transfer function in the parabolic flow model was calculated numerically, and was found to be somewhat narrower than the uniform flow model, especially when the resolution parameter λ_c is larger than unity.

A similarity rule has been derived which states that the transfer function is determined solely by λ_c . This rule is mathematically inexact, but is expected to be valid to good accuracy in practical situations. In applications, this similarity rule will be useful in choosing the operating parameters for optimal performance.

A prototype classifier was constructed and the mass distribution of $0.309\ \mu\text{m}$ monodisperse particles was measured with this device. The locations of maxima in the experimental spectra were found to agree fairly well with the theory, which has verified the feasibility of this method.

One of the favorable features of this method is that the classification performance is insensitive to the instability and inhomogeneity of the aerosol flow in the operating space. The shape of the transfer function will be distorted to some extent by these imperfections of the flow field, but its center, s_c , will not be shifted in principle. This feature will facilitate designing and constructing this type of classifier.

Acknowledgements—The authors are grateful to Dr G. W. Mulholland, National Institute of Standards and Technology (NIST), and Prof. Y. Kousaka, University of Osaka Prefecture, for valuable discussions. Part of this work was done while one of the authors (K. E.) stayed at NIST as a guest researcher. He would like to thank Dr R. J. Lundegard, for his encouragement during this work.

REFERENCES

- Abed-Navandi, M., Berner, A. and Preining, O. (1976) In *Fine Particles* (Edited by Liu, B. Y. H.), p. 447. Academic Press, New York.
- Allen, M. D. and Raabe, O. G. (1985) *Aerosol Sci. Technol.* **4**, 269.
- Beeckmans, J. M. (1979) In *Aerosol Measurement* (Edited by Lundgren, D. A. *et al.*), p. 56. Univ. Press Florida, Gainesville.
- Gerber, H. E. (1979) *ibid.*, p. 36.
- Hagwood, G., Coakley, K. J., Negiz, A. and Ehara, K. (1996) To be published in *Aerosol Sci. Technol.*
- Hewitt, G. W. (1957) *Trans. Am. Inst. Elect. Engrs* **76**, 300.
- Hochrainer, D. (1971) *J. Colloid Interface Sci.* **36**, 191.
- Knutson, E. O. and Whitby, K. T. (1975) *J. Aerosol Sci.* **6**, 443.
- Kousaka, Y., Okuyama, K., Shimada, M. and Ohshima, H. (1988) *J. Aerosol Sci.* **19**, 501.
- Landau, L. D. and Lifshitz, E. M. (1963) *Fluid Mechanics (Course of Theoretical Physics, Vol. 6)*, p. 57. Pergamon Press, Oxford.
- Liu, B. Y. H., Pui, D. Y. H. and Kapadia, A. (1979) In *Aerosol Measurement* (Edited by Lundgren, D. A. *et al.*), p. 341. Univ. Press Florida, Gainesville.
- Marple, V. A. and Willeke, K. (1979) *ibid.*, p. 90.
- Masuda, H., Hochrainer, D. and Stöber, W. (1979) *J. Aerosol Sci.* **10**, 275.
- Masuda, H., Gotoh, K. and Orita, N. (1993) *J. Aerosol Res. Japan* **8**, 325 (in Japanese).
- Prodi, V., Melandri, C., Tarroni, G., DeZaiacomo, T., Formignani, M. and Hochrainer, D. (1979) *J. Aerosol Sci.* **10**, 101–119.
- Schlichting, H. (1962) *Boundary Layer Theory*, 2nd English Edition, p. 171. McGraw Hill, New York.
- Sinclair, D., Countess, R. J., Liu, B. Y. H. and Pui, D. Y. H. (1979) In *Aerosol Measurement* (Edited by Lundgren, D. A. *et al.*), p. 544. Univ. Press Florida, Gainesville.
- Stöber, W. (1976) In *Fine Particles* (Edited by Liu, B. Y. H.), p. 351. Academic Press, New York.
- Stöber, W. and Flachsbarth, H. (1971) *J. Aerosol Sci.* **2**, 103.
- Stevenson, H. J. R. and Preining, O. (1960) *J. Air Pollution Control Assoc.* **10**, 378.
- Talley, D., Raabe, O. G. and Mewhinney J. A. (1979) In *Aerosol Measurement* (Edited by Lundgren, D. A. *et al.*), p. 29. Univ. Press Florida, Gainesville.
- Tillery, M. I. (1979) *ibid.* p. 3.
- Whitby, K. T. (1976) In *Fine Particles* (Edited by Liu, B. Y. H.), p. 584. Academic Press, New York.